Best Paper Award

The following paper was selected by the Awards Subcommittee of the International Symposium on Superalloys as a co-winner of the Best Paper Award for the Ninth Symposium. The selection was based on the following criteria: originality, technical content, pertinence to the superalloy and gas turbine industries and clarity and style.

Novel Casting for Single Crystal Gas Turbine Components

M. Konter, E. Kats, and N. Hofmann

A NOVEL CASTING PROCESS FOR SINGLE CRYSTAL GAS TURBUNE COMPONENTS

M. Konter, E. Kats*, N. Hofmann*

ABB ALSTOM Power, CH 5401 Baden, Switzerland;
*ABB ALSTOM Power Technology, CH 5405 Baden-Dättwil, Switzerland

Abstract

The novel directional solidification process was developed at ABB for the manufacturing of large single crystal components. In addition to the radiation cooling, typical for the conventional Bridgman technology, an inert gas is injected directly below the furnace baffle. Experiments show that for the Gas Cooling Casting (GCC) process the heat transfer coefficients are significantly higher compared to those in the Bridgman process and are similar to the best LMC practice.

Introduction

The drive to higher efficiency land-based gas turbines has resulted in wide use of single crystal technology. Single crystal and directionally solidified blades are traditionally produced by a casting technique known as the Bridgman process.

In this process, the superalloy is molten in a vacuum chamber and poured into a heated ceramic mould. The mould is mounted on a copper chill, and the whole assembly is withdrawn from the melting/heating chamber into a cooling chamber so as to produce a vertical temperature gradient in the solidified (mushy) zone of the casting. While the first 40–60 mm of the casting are efficiently cooled by conduction of heat through the water-cooled bottom copper chill, the main part of the large IGT parts is cooled by a radiation heat transfer from the mould sides towards water-cooled vacuum chamber walls. The temperature gradient induces directional solidification, and either a single crystal seed or a complex spiral "pig tail" ensures that the blade is produced as a single crystal.

The economics of the single crystal casting process are directly related to the rate of grain defect production. Grain defects such as freckles, strain and spurious grains, and low angle boundaries limit the production yield. The tendency to grain defect formation increases as the size and mass of the component increases. This is due to the difficulty of maintaining a reasonably high temperature gradient at the liquid-solid metal interface by the heat radiation transfer in vacuum. This is illustrated by the fig.1, which schematically shows the defect–free region in thermal gradient – solidification rate coordinates. Improvement of casting yield for large SX blades has only a limited potential within an existing process design. Demand for a more efficient single crystal casting process led to rediscovery of the Liquid Metal Process (LMC) as well as development of the new technique, the Gas Cooling Casting (GCC).

Heat flux analysis

The conventional industrial single crystal casting process (so - called Bridgman technique) is described in the patent [1]. The mould is being preheated to the temperature above the metal liquidus and after the pouring of the molten metal is removed at a controlled withdrawal rate from the heating furnace to the cooling chamber. The heating furnace during withdrawing process is maintained at full power. The heating and the cooling chambers are separated by the baffle in order to maintain the thermal gradient as high as possible. The ceramic mould is placed on the chill plate, which is the part of withdrawing mechanism. In the beginning of the solidification process the heat is removed by conduction along the ingot to the chill plate. However, for large castings, conduction is mostly limited to the starter or a pig – tail, and the main part of the component solidifies by the process, where the predominant heat loss is a combination of:

- conduction through the portion of mushy and solidified metal placed above the baffle (in a case of a liquidus line being above the baffle) with the heat exchange coefficient α_{cm},
- heat transfer from the metal through the vacuum gap between the solid metal and the ceramic shell to the mould inner surface with the heat exchange coefficient α_{gap} (the metal – shell radiation);
- conduction through the porous ceramic shell mould to the mould outer surface with the heat exchange coefficient α_{cmd}, (more exactly, the heat transfer process here is a combination of the conduction with a

Superalloys 2000
Edited by T.M. Pollock, R.D. Kissinger, R.R. Bowman,
K.A. Green, M. McLean, S. Olson, and J.J. Schirra
TMS (The Minerals, Metals & Materials Society), 2000

radiation at pores, depending on the pore size and morphology);
- radiation heat transfer from the mould surface to the colder surroundings (water-cooled chamber walls) with the heat exchange coefficient α_ρ.

With certain approximation, the heat flux in the multistage cooling process can be described using a combined heat transfer coefficient α in the Newton heat transfer law

$$Q = \alpha (T - T_0), \qquad \{1\}$$

For an estimation of the potential of various casting processes, the α is defined as:

$$1/\alpha = 1/\alpha_{cm} + 1/\alpha_{gap} + 1/\alpha_{cmd} + 1/\alpha_r, \qquad \{2\}$$

though this approach is a stationary 1-D heat flux approximation, assuming that heat fluxes through the gap, mould and from the mold surface are the same (better would be consideration of steps in the heat flux rather than α).

For a large blade:

$$\alpha_{cm} = \lambda_m / \delta_m = 25 / 0.025 = 1000 \ W/m^2K, \qquad \{3\}$$

$$\alpha_{cmd} = \lambda_{md} / \delta_{md} = 1.5 / 0.012 = 125 \ W/m^2K, \qquad \{4\}$$

where λ_m and λ_{md} are the thermal conductivity of metal and mould, δ_m and δ_{md} are the thickness of the portion of metal described above (taken as 25 mm) and the mould thickness (12 mm) respectively (see also measurements reported below);

$$\alpha_{gap} = 4\varepsilon_{eff} \sigma T^3 = 4(1/(1/\varepsilon_1 + 1/\varepsilon_2 - 1)) \sigma T^3$$
$$\alpha_{gap} = 230 \ W/m^2K, \qquad \{5\}$$

and

$$\alpha_r = \sigma(\varepsilon_3 T_1^4 - \varepsilon_4 T_0^4)/(T_1 - T_0) = 120 \ W/m^2K, \qquad \{6\}$$

where σ is the Steffan - Boltzmann constant, ε_1, T; ε_2, ε_3, T_1 and ε_4, T_0 are the emissivity and the temperature of the metal surface; mould inner and outer surface and the absorption and the temperature of the surroundings respectively ($\varepsilon_1 = 0.4$, $\varepsilon_2 = 0.5$, $\varepsilon_3 = \varepsilon_4 = 0.45$, $T = 1580K$, $T_1 = 1500K$, $T_0 = 400K$).

Then,

$$1/\alpha = 1/1000 + 1/230 + 1/125 + 1/120 \qquad \{7\}$$

$$\alpha \text{ (Bridgman process)} = 46 \ W/m^2K. \qquad \{8\}$$

Equation {7} shows that heat transfer process in Bridgman technique is limited by the heat exchange between the mold and environment but also by the mold and the vacuum gap.

The relatively low heat exchange in the Bridgman process limits the withdrawal speed w and the solidification front velocity v. Low v results in the coarse dendrite structure, followed by various grain defects, such as freckles and internal grains [2]. If withdrawal speed is increased in order to increase v, the solidification front moves into the cooling zone and the ratio between transverse and longitudinal temperature gradient on the liquidus front Gt/Gl exceeds the critical value range of 0.2-0.3, typical to formation of the spurious grains [3]. Often, the only remaining effective way to increase the yield is reduction in number of parts per mold, which increase the ε_3 in the equation {6}. This, however, significantly reduces process capacity and increases costs per part.

In order to increase the process effectiveness, several techniques have been developed. Patent [4] discloses a casting process in which the mould is immersed in a bath with liquid metal coolant (LMC process). The LMC process is described elsewhere [5-7] and is schematically shown on fig.2. The modification of this process with molten aluminum as a coolant is currently widely used in Russia. Though, when liquid aluminum is used, the distance between the solidification front and the heat extraction level is slightly increased, the last part of the equation {2} nearly disappears, being replaced by very high heat transfer coefficient of convection in the liquid metal. Floating baffle reduces the distance between the solidification front and the heat extraction level (in our example – LMC Sn). Now for a large blade:

$$1/\alpha = 1/\alpha_{cm} + 1/\alpha_{gap} + 1/\alpha_{cmd} + 1/\alpha_{lmc}. \qquad \{9\}$$

$$\alpha_{cm,baffle} = \lambda_m / \delta_m = 25 / 0.03 = 830 \ W/m^2K. \qquad \{10\}$$

$$\alpha_{cm,\ float.baf.} = \lambda_m/\delta_m = 25/0.022 = 1136 \ W/m^2K \qquad \{11\}$$

$$\alpha_{lmcAl} = Nu\,\lambda_{Al} / L = 11500 \ W/m^2K. \quad \{12\}$$

$$\alpha_{lmcSn} = Nu\,\lambda_{Sn} / L = 6500 \ W/m^2K. \quad \{13\}$$

where Nu is the Nusselt criteria, calculated using a combination of the Prandtl criteria and the Grassgoff criteria, and L is the length of the dipped mold. The thermal conductivity of the mold only slightly depends from the temperature in the temperature range 500° – 950°C, and the α_{cmd} for the mentioned processes varies within +/- 5%, with mold thermal conductivity slightly lower at higher temperature (Al process).

$$1/\alpha_{lmcAl} = 1/830 + 1/230 + 1/120 + 1/11500 \quad \{14\}$$

$$1/\alpha_{lmcSn} = 1/1136 + 1/230 + 1/125 + 1/6500 \quad \{15\}$$

$$\alpha\,(\text{LMC Al}) = 72 \ W/m^2K. \quad \{16\}$$

$$\alpha\,(\text{LMC Sn, float.baffle}) = 75 \ W/m^2K. \quad \{17\}$$

Back to the heat flux in equation {1}, we can compare the potential effectiveness of various casting techniques:

$$Q\,\text{Bridgman} = 46\ (1700 - 400) = 60\ kW/m^2 \quad \{18\}$$

$$Q\,\text{LMC Sn} = 75\ (1700 - 550) = 86\ kW/m^2 \quad \{19\}$$

$$Q\,\text{LMC Al} = 72\ (1700 - 950) = 54\ kW/m^2 \quad \{20\}$$

where 1700K is the metal temperature on solidification front and 350K, 550K and 950K is the temperature of the "heat sink" in Bridgman process (cooled furnace walls), and in LMC process with liquid Sn and Al correspondingly.

One should anticipate, that despite an elimination of a bottle neck in the overall heat transfer process – the heat resistance of the vacuum chamber, the effectiveness of LMC process is limited by heat resistance of the mould and, to smaller extent, by heat resistance of the vacuum gap. On the other hand, in the real LMC process, especially one with the floating baffle, the real heat flux is quite close to the calculated potential. In a contrast, in Bridgman process a cooled mold faces significant heat input from the heat chamber through the baffle opening and from the central feeder/mould holder and adjoining parts in the cluster. This explains why, without having advantage in the cooling potential, the Al – LMC process in practice often shows better gradients compared to the Bridgman technique.

The novel directional solidification technique, developed by ABB ALSTOM Power, is targeted to significantly improve all three meaningful heat transfer processes: heat transfer through the gap, through the mold and heat remove from the mold surface. In the Gas Cooling Casting process (GCC) [8], in addition to the radiation cooling, the mould surface sees an impingement cooling by the inert gas, injected at high velocity directly below the furnace baffle (fig.3). In GCC process heat is effectively removed from the mold outer surface by high velocity gas flow and, additionally, by radiation heat transfer (mold surface is colder compared to the Bridgman process). The average heat transfer coefficient of the impingement gas cooling by argon – helium mix was conservatively taken as 510 W/m^2K (for an optimized process a higher value can be achieved):

$$\alpha_{GCC} = \alpha_{gas} + \alpha_r = 510 + 90 = 600 \ W/m^2K. \quad \{21\}$$

Additionally, the high-pressure gas jet in the process of impingement cooling fills the porous mold and the vacuum gap with gas, predominantly helium, which increases their heat conductivity. The following values have been measured:

$$\alpha_{cmd} = \lambda_{md} / \delta_{md} = 2.0 / 0.012 = 166 \ W/m^2K, \quad \{22\}$$

$$\alpha_{gap} = 300\ W/m^2K \quad \{23\}$$

Then,

$$1/\alpha_{GCC} = 1/830 + 1/300 + 1/166 + 1/600 \quad \{24\}$$

$$\alpha_{GCC} = 81 \ W/m^2K. \quad \{25\}$$

$$Q\,GCC = 81\ (1700 - 450) = 101\ kW/m^2 \quad \{26\}$$

From the heat flux point of view, GCC process has the highest potential among the considered techniques, followed by LMC with Sn bath and a floating baffle, while the LMC process with Al as a cooling media has no advantage compared to the Bridgman technique. However, as was already pointed out, in the casting practice, especially when multi-component mold is used, GCC as well as Bridgman process can not realize the full potential due to the additional radiation heat input. Industrial effectiveness of the various techniques is assessed in the Table 1 based on the casting process modeling results. The dendrite arm spacing (DAS), measured after industrial casting trials on large cored blades, confirms this ranking. Note, that an advanced furnace design, such as internal baffle and central heat sink [9], help to bring industrial effectiveness of the Bridgman (as well as GCC) process closer to the theoretical values.

Table 1. Assessment of the relative cooling effectiveness for casting techniques

Process	Bridgman	GCC	LMC Sn	LMC Al
Physical potential of the cooling effectiveness	1	1.7	1.45	1
Estimate of cooling effectiveness in an industrial process	0.6	1.5	1.5	1
DAS, μm for large cored blades; low airfoil.	430	320	(330) [10]	360

Experimental procedure

The GCC feasibility study and benchmarking of LMC and Bridgman casting processes have been carried out at ABB Corporate Research in an industrial-size furnace UVNK-8P, fully automated and modified for each of the mentioned techniques (fig.4). The furnace was equipped with induction crucible, two graphite resistance heaters, baffle and pull-down rod with a hanger for mould. Additionally, the bath with molten Al (LMC) or the nozzle system with gas supply (GCC) was placed below the baffle. The distance between Al surface and the baffle was varied from 20 to 40 mm. The distance between the baffle level and a projection of nozzle centerline on the mould surface was varied from 0 to 100 mm. The clusters of 2 shrouded solid blades, 240 mm in length and with airfoil wall thickness from 3 to 8 mm were cast with each technique (fig. 5). Alumina – based molds have been produced by the standard stucco-and-slurry technique with some of LMC molds additionally wire supported. The single crystal structure was provided by single crystal seeding technique and a 12 - 15 mm. long grain selector. The alloys used in experiments were CMSX-4 [11] with liquidus temperature 1410°C and MK-4 [12] with liquidus temperature 1407°C. Heaters temperature was carried at 1550°C for the upper and 1600°C for the lower heater. Al bath temperature was carried in the range of 680 – 700°C and the gas temperature was 100 – 170°C on the nozzle exit. As a gas media an Ar, He and their mixture in various proportions have been tested. For the process control additional thermocouples have been placed on mold, in the LMC bath, on the gas nozzles, in the heater chamber, on the inner wall of the vacuum chamber, on gas exhaust in front of and behind the intercooler.

After grain structure etching and visual inspection the blades have been cut in 2 locations in the airfoil and 2 locations in the root. Some of blades have been heat treated prior to etching. The heat treatment cycle for both alloys consisted of multi-step solutioning with the maximum cycle temperature of 1310°C [13], precipitation heat treatment at 1140°C and aging at 870°C. The primary dendrite arm spacing, porosity, γ'-phase size, concentration profiles of elements have been investigated using standard procedures of etching, optical and scanning (SEM) microscopy, EDX and VDDX microprobe analysis.

The fluid dynamic and heat transfer optimization of the GCC process has been carried on in a large vacuum chamber, where a 1:1 model of the induction heating chamber of industrial casting furnace was installed. The influence of various GCC process parameters on heat transfer values and distribution was studied on plaster model of the casting mold with 7 of GT24 low pressure 1st row blades. Heat transfer has been measured using thermocouples and the IR-scanner AGA-780. The thermocouples have been installed into the plaster model on various depths, so at the beginning the time at temperature, necessary for stabilization of the temperature profile has been defined. The plaster model has been heated up to 800°C for 30 min. Then the furnace with attached baffle and the nozzle ring beneath was lift up the certain height to section, where the measurements of heat transfer should be carried out. Than, the steady gas flow through the nozzles was activated. The recording of thermo - images by IR-scan and temperature by thermocouples was conducted prior and during the gas jet action, which allowed to use (with certain limitations) the heat conduction equation for a semi-infinite body with type III boundary conditions to describe the convective heat flux. The heat transfer coefficient was determined as follows:

$$\alpha = U\lambda / (a\tau)^{1/2}, \text{ W/m}^2\text{K}, \quad \{27\}$$

where λ and a are heat and temperature conductivity of plaster, τ - the time of jet action onto the model surface and U is the non-dimensional parameter, determined from the equation:

$$(T_t - T_0) / (T_s - T_0) = 1 - e^{U2} (1 - 2/\sqrt{\pi} \int_0^U e^{-t2}\, dt), \quad \{28\}$$

where T_t, T_0 and T_s are temperature of the mold surface at the moment t, initial mold temperature and stagnation temperature of the cooling gas.

The ceramic mold heat diffusivity was measured on a shell created by ACCESS e.V. (Aachen, Germany) by a laser flash method at the Institute of Ceramic Components (RWTH, Aachen). The measurement was performed under vacuum, air (1 bar), argon (150 mbar), helium (150 mbar) and a helium/argon mixture (20% He/ 80% Ar, 150mbar). The thermal diffusivity was measured in steps of 100°C in a temperature range between 20°C and 1600°C. At each temperature the diffusivity was measured 4 times and then averaged. The measurement error was approximately 3%.

Measurement of thermal diffusivity described as:

$$\alpha = \lambda/(\rho c_p) \quad \{29\}$$

[Heat Conductivity / (Density * Heat Capacity)]

The mold ceramic was Al_2O_3 with SiO_2 slurry. Samples from the rough and smooth surface of the shell, ϕ = 12.7 mm, with a thickness of 3 mm, porosity 30%. Samples were covered with graphite to avoid transmission of the laser.

Mold conductivity in the gas cooling process

The thermal diffusivity of the ceramic shell mould was measured in a temperature range from 20°C to 1600°C. The purpose of this measurement was to study the impact of helium and argon on the thermal conductivity of the shell. The thermal diffusivity of the shell is conductivity to the amount of heat, which will be transported through the shell in the Bridgman process. The increase in the thermal diffusivity increases the thermal gradient and cooling rate.

The thermal conductivity is influenced by microstructure discontinuities such as cracks or pores, which will interfere with the direct flow of heat. In the case of cracks the volumetric heat capacity is maintained such that the heat storage capacity is unaffected.

Pores, in contrast, will lower the volumetric heat capacity in direct proportion to the volume fraction of the pores. Additionally the pore size and volume indicates that the specific heat is not affected by the combined effects of pore content and accompanying changes in the crystallographic phase content [14]. Although the volumetric heat capacity decreases with decreasing density, the *heat capacity per unit mass* of shell material is independent of the pore content.

On the other hand the thermal conductivity is strongly affected by the microstructure discontinuities like crack and pore size and distribution. There has been systematic experimental work on the methodological problems of determining the thermal conductivity of refractories [15]. Particularly the presence or absence of gas in the pores and cracks significantly influence the thermal conductivity. Most measurements on thermal conductivity are performed under atmospheric conditions and do not represent the thermal conductivity of porous ceramics under vacuum conditions like in a Bridgman process.

Figure 6 shows the thermal conductivity of the smooth surface of the shell. The thermal conductivity of the rough surface is approximately 1% higher than the smooth surface (not shown in the plot). The thermal conductivity of the shell in air at 1 bar is app. 50 % higher than the vacuum conductivity. For argon and the 80% argon + 20% helium mixture at 150 mbar the thermal conductivity is 30 % higher than in the vacuum. The use of pure helium at 150 mbar gives a limited improvement of the thermal conductivity compared to the gas mixture, from plus 30% over the vacuum in gas mix to plus 43 % compared to vacuum for the pure helium in the temperature range 800°- 1200°C.

The benefit of the GCC process is a significant improvement in the shell thermal conductivity (shell temperatures around 1000°C for GCC) of 30%. Consequently the heat flow, the cooling rate and the temperature gradient are increased by 30%.

Figure 7 shows the ratio of thermal conductivities between shell exposed to a given gas and vacuum thermal conductivity (conventional process). The figure illustrates that air has a decreasing influence on thermal conductivity with increasing temperature. Argon and helium in the temperature range between 800°C and 1200°C show the highest impact on the thermal conductivity of the shell. This is exactly the temperature range of the shell situated under the baffle in the casting process.

Influence of gas flow parameters

The following parameters have been optimized using fluid dynamic and heat transfer experiments:

- gas velocity in the jet;
- total jet pressure;
- nozzle diameter;
- level of initial turbulence;
- gas pressure in the vacuum chamber;
- gas volume;
- gas composition;
- distance from the nozzle to the mold;
- position of the jet centerline on the mold;
- jet inclination angle.

Jet inclination

Fig. 8 shows results on inclination angle experiments. The jet normal to the mold surface results in a relatively low cooling effectiveness due to vortex formation from reflected gas and poor gas flow along the profile. Effectiveness of the inclined jet is much higher, with a maximum in a wide range of inclination angles from 30° to 60°, showing heat transfer coefficient two times higher compared to one for a gas jet normal to the surface.

Experiments have demonstrated, that at inclination angle from 30° to 60° the gas flow follows the concave and convex profile of the cored large IGT blade mold. Almost no flow separation was detected even in the leading edge area. Distribution of heat transfer coefficients along the mold profile, measured with IR-scanner, was very homogeneous with α max / α min < 3. Taking into account significant homogenization of the temperature fields across the mold thickness (due to the low thermal conductivity of ceramic) the cooling inhomogenity along the blade profile is insignificant on the metal surface. Analysis of blade dendrite morphology after casting confirms this point.

Distance to the mold

Fig. 8 shows also an influence of distance from the nozzle to the mold on the cooling effectiveness. At selected flow parameters (velocity, pressure at the nozzle and in the chamber), cooling is still very effective even at distance up to 150 mm., with optimum values up to 100 mm.
Interestingly, the measured curve for heat transfer coefficient α vs. distance from the nozzle to the mold shows a significant difference compared to the curve which would be theoretically expected for vacuum from the law $\alpha \approx 1/x$ (where x is the distance to the mold). This is due to additional gas volumes, involved by turbulence in the gas jet from the chamber atmosphere.

Material structure

Macrostructure of the blades cast in various techniques shows a consistent difference in dendrite arm spacing, in porosity level and an insignificant difference in volume fraction of residual eutectic. Figure 9 illustrates the typical macrostructure after Bridgman, LMC Al and GCC process for the airfoil cross-section close to the platform. Figure 10 shows measurement results for dendrite arm spacing. The lower airfoil area is the most representative for assessment of the relative temperature gradient in vertical direction using the primary DAS parameter. This zone is characterized by stabilized solidification front velocity, quite close to the withdrawal speed. Comparison of GCC, LMC and Bridgman trials, with taking into account difference in withdrawal speed, confirms an advantage of GCC process.

Secondary and tertiary dendrite arms, strongly extended in one preferential direction on the figure 10 reflect a pronounced transverse gradient in Bridgman and, especially, LMC casting trials. In both trials withdrawal speed was kept as high as possible (5 mm/min and 8 mm/min respectively) in order to prevent freckle – induced grain defects. This, however, results in shifting solidification front beneath the baffle, strong inclination of the front line and, in a turn, fluctuation induced grain defects. This point is illustrated on the defect map on the figure 1. GCC process, in contrast, shows almost an ideal dendrite shape, typical for high longitudinal to transverse temperature gradient ratio and wide process window.

GCC process results (as a consequence of higher cooling rate and high longitudinal to transverse temperature gradient ratio) in a lower porosity. Comparison of porosity area fraction for three casting techniques is given in the Table 2.

Table 2. Area fraction of porosity.

Process	Bridgman	LMC-Al	GCC
Upper airfoil, %	0.32	0.18	0.06
Lower airfoil, %	0.24	0.19	0.08

More important for component life is, however, the maximum pore size. Pore size distribution is illustrated by figure 11. The largest detected pore had 70 mm, 60 mm and 45 mm maximum size for Bridgman, LMC and GCC process correspondingly. In general, GCC process results in much smaller amount of large pores, which provides a good potential for an extended fatigue life.

The area fraction of residual eutectic in as-cast condition does not show significant difference between various casting techniques (fig. 12). Finer morphology of eutectic islands after GCC process is beneficial for solutioning heat treatment.

There was no significant difference between casting techniques in dendritic segregation of elements in as-cast condition (fig. 13). A slight beneficial trend in segregation of Re may, however, result in better homogenization during solutioning heat treatment and, therefore, higher structure- and phase- stability during the long time high temperature operation.

Both LMC-Al and GCC process are characterized by significantly finer γ' –phase morphology in as-cast condition compared to the conventional casting technique (fig. 14). The γ' –size is determined by the cooling rate in the temperature range below γ' – solvus. In this range the liquid Al bath provides effective cooling, while radiation heat transfer from the mold is poor. With respect to GCC process, the low-temperature part of the casting is not directly exposed to the gas jets, however, to our opinion, the gas – filled mold and gap, as well as convection cooling through the chamber, result in the cooling rate comparable to LMC. Finer γ' – structure is potentially beneficial first of all for vane applications, if vanes are used in as-cast or partially solutioned condition in order to avoid recrystallization. Too high cooling rate at lower temperatures, however, results in residual stresses in casting and promotes recrystallization during solution heat treatment.

Casting process application

Industrial demand for the directional solidification process with an increased cooling rate is obvious. Wide application of the LMC process, however, requires high initial investments and, for the tin process, solution of certain mold technology problems. Gas cooling casting process does not request a replacement or a significant modification of the existing Bridgman equipment. The manifold with nozzles and attached gas supply can be easily installed in any DS furnace and investments in an additional gas and control equipment are marginal. The modified furnace always can function in the Bridgman process mode with only the manifold removed.

With regard to casting technology, experiments show that a flexible control over gas parameters during the withdrawing

process allows optimization of casting structure in the most critical areas, such as shrouds and platforms. The typically higher process withdrawal speed also improves the plant economics.

Summary

The novel gas cooling casting process has been developed for production of single crystal and directionally solidified gas turbine components. The process has been validated on semi-industrial furnace and directly compared to the conventional and LMC single crystal casting technique. Theoretical analysis of heat flux during the various SX casting processes show a significant advantage of the gas cooling over existing techniques. Improvement in a heat flux during the solidification comes from the direct gas jet impingement cooling as well as from improvement in the mold heat conductivity. The sensitivity analysis of the heat transfer in the GCC process from various process parameters and gas system design had been performed on the test rig and allowed to design the gas system for industrial furnace. Casting trials show doubled temperature gradient compared to conventional Bridgman technique. Micro – and macrostructure of the GCC – cast blades show certain potential for easier post – processing and longer fatigue life.

References

1. F.L. Versnyder: US Patent No. 3 260 505, 1966.
2. T.M. Pollock, W.H. Murphy: The Breakdown of Single-Crystal Solidification in High Refractory Nickel-Base Alloys, Met. Trans., v. 27A, Apr. 1996
3. E. Kats, S. Korjakin, A. Amiljanchik, E. Spiridonov: Thermal process during formation of a SX structure in superalloys. Proc. Of the 1st International Heat-resistant Material Conference, 23 – 26 Sept. 1991, Fontana WI, 1991.
4. J.G. Tschinkel, A.F. Giamei and B.H. Kear: US Patent No. 3 763 926, 1973.
5. R.F. Singer: Directional and Single Crystal Solidification Using LMC. 3rd Symposium on Advanced Technologies and Processes for Metals and Alloys, Hanau, ALD Vacuum Technologies, 1995.
6. M. Konter, N. Hofmann, C. Tönnes, M. Newnham: Influence of a Casting Process with High Cooling Rate on Structure and Properties of SX and DX Componets for Industrial Gas Turbines. 3rd Symposium on Advanced Technologies and Processes for Metals and Alloys, Hanau, ALD Vacuum Technologies, 1995.
7. F. Hugo, U. Betz, J. Ren, S.-C. Huang, J. Bondarenko, V. Gerasimov: Casting of Directionally Solidified and Single Crystal Components Using Liquid Metal Cooling (LMC). International Symposium on Liquid Metal Processing and Casting, Santa Fe, VMD – AVS, 1999.
8. E. Kats, M. Konter, V. Lubenets, J. Rösler: US Patent No 5 921 310, 1999.
9. F. Hugo, R. Schumann, W.T. Carter Jr.: Advanced Vacuum Metallurgical Processes and Equipment for Gas Turbine Materials and Components. Gorham's Int. Business Conference, Tampa, Gorham Advanced Materials Inc., 1998.
10. J. Grossmann, J. Preuhs, W. Esser, R. Singer: Investment Casting of High performance Turbine Blades by Liquid Metal Cooling – A Step Foreward Towerds Industrial Scale Manufacturing. Proc. Of the 1999 int. Symposium on Liquid metal processing and Casting, Santa Fe, NM, Feb. 1999
11. K. Harris, L. Erickson: US Patent No 4 643 782, 1987.
12. M. Konter, C. Tönnes, M. Newnham: US Patent No 5 759 301, 1998.
13. M. Konter: US Patent No 5 882 446, 1999.
14. M.V. Swain, L.F. Johnson, R. Syed, D.P.H. Hasselman: Thermal diffusivity, heat capacity and thermal conductivity of porous partially stabilized zirconia, Journal of Material Science Letters 5, 1986, p. 799-802
15. V.V. Pustovalow: Thermal Conductivity of Refractory Materials, Translated from Russian, NASA Accession Number N71-15034 1971, Printed and Published by INSDOC, Delphi-1

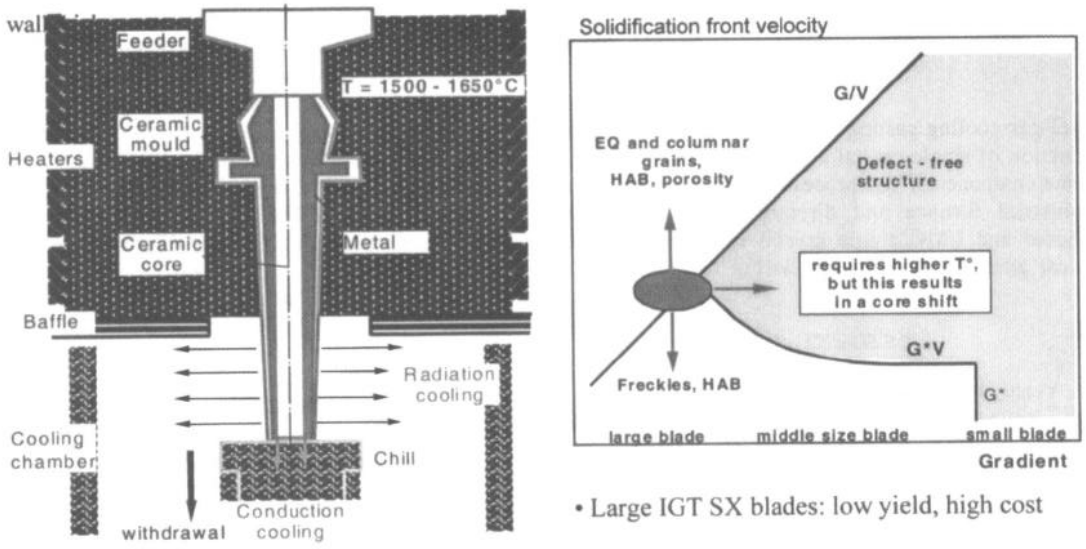

Fig. 1: Bridgman process with grain defect map.

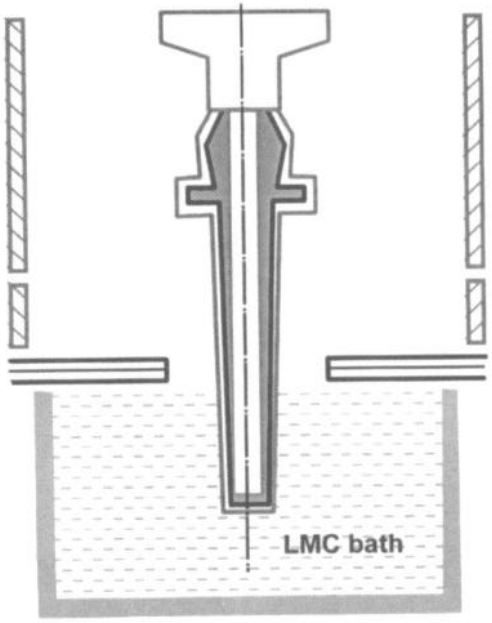

Fig. 2: Liquid metal casting process

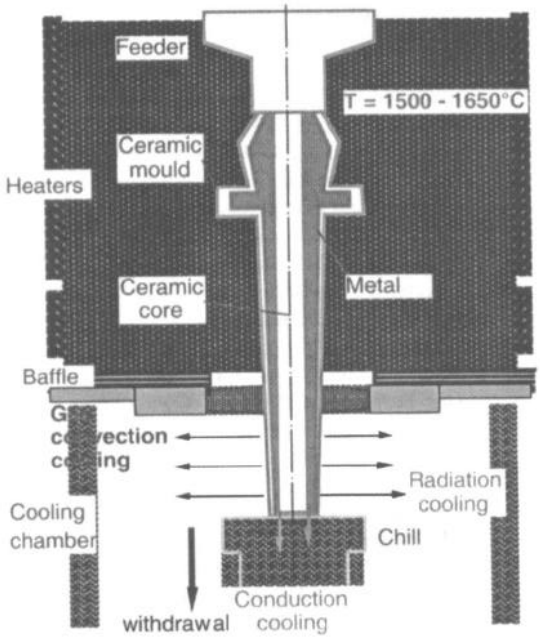

Fig.3: Gas cooling casting process

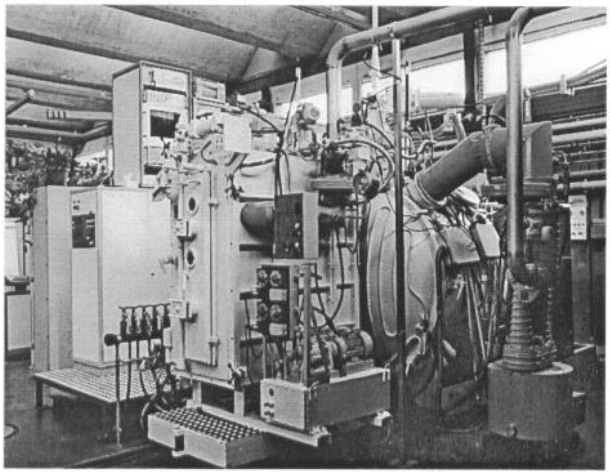

Fig. 4: Casting furnace at ABB ALSTOM Power used for trials with various cooling media.

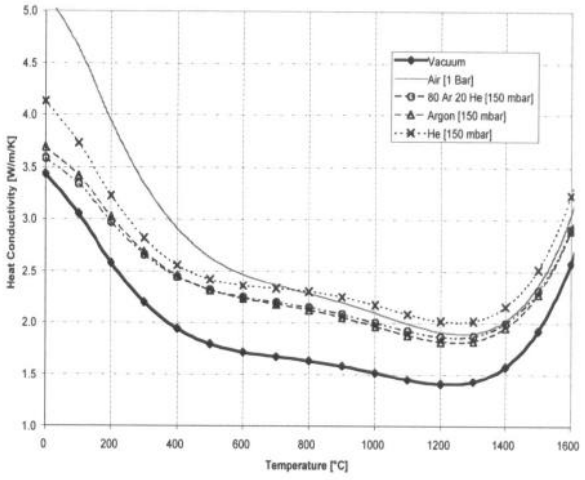

Fig. 6: Thermal conductivity of shell material exposed to various gases.

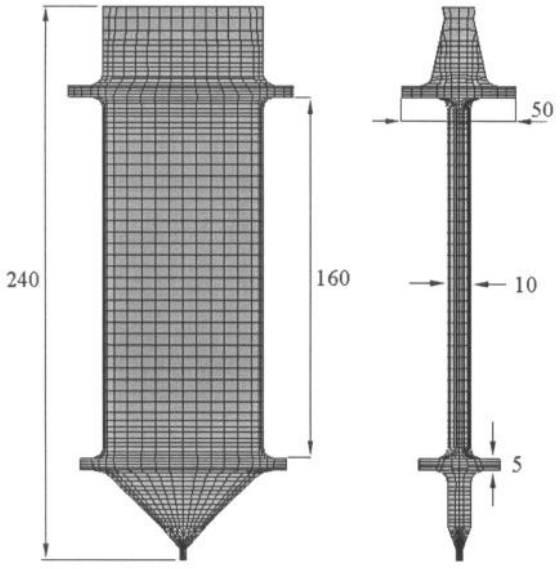

Fig. 5: Solid shrouded blade used for the initial casting experiments.

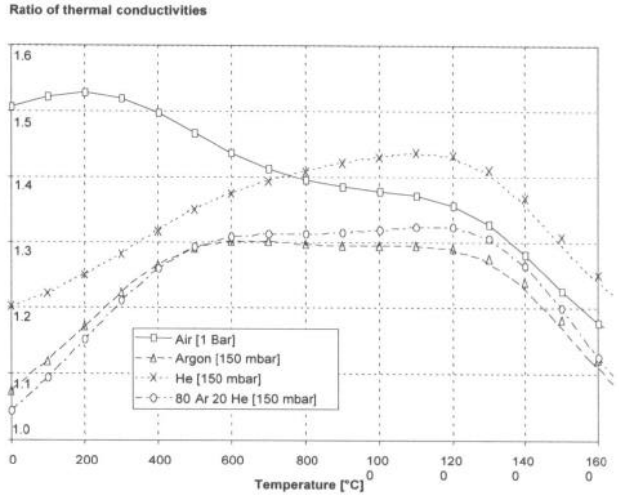

Fig. 7: Ratio of shell conductivity for mold exposed to a given gas to the conductivity of mold in vacuum.

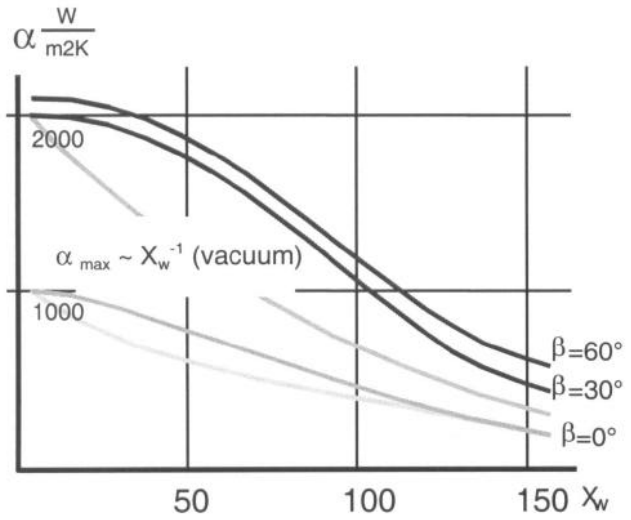

Fig. 8. Influence of a distance between the nozzle and the mold (**X**w, mm) and of the jet inclination (β) on the heat transfer coefficient α (Ar/He mix).

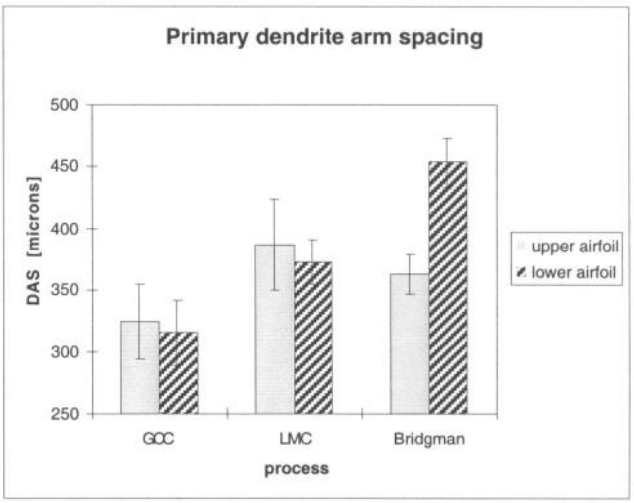

Fig. 9. Primary dendrite arm spacing after different casting processess.

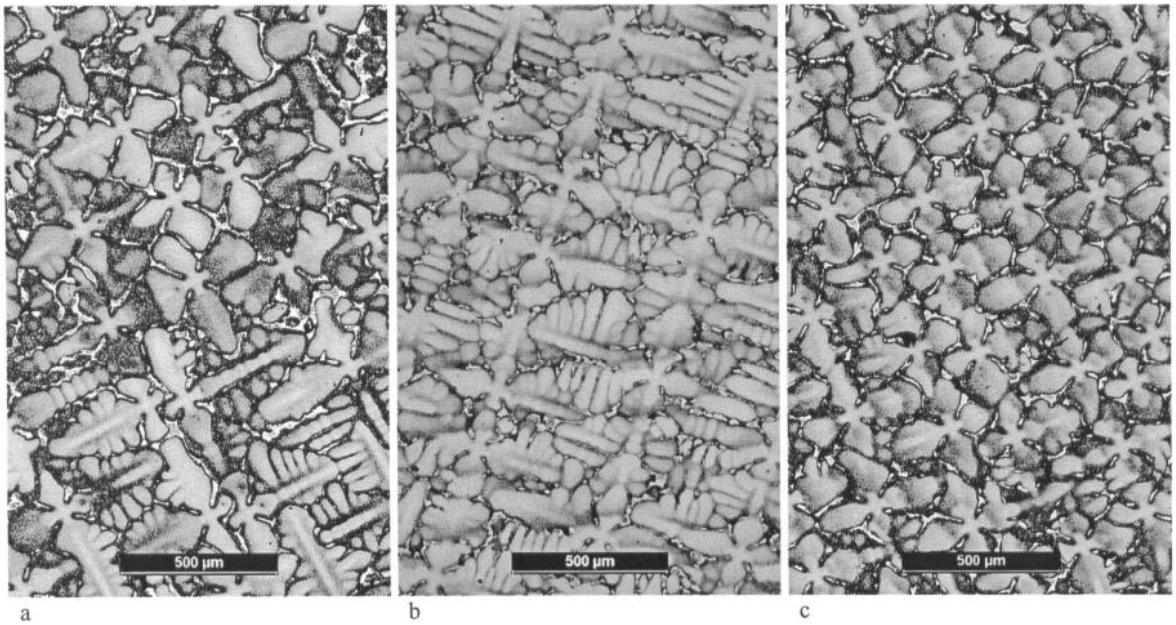

a b c

Fig. 10 . Macrostructure of SX alloy (MK4) in as cast condition after Bridgman (a), LMC – Al (b) and GCC (c) casting, lower airfoil.

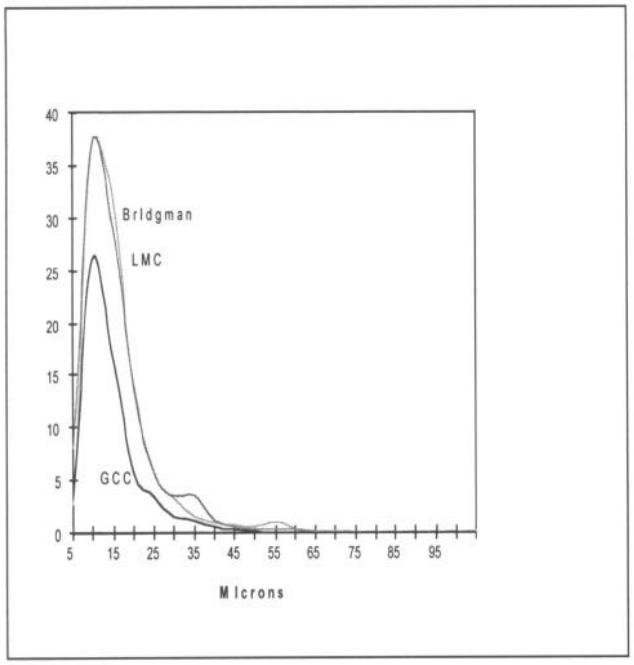

Fig. 11: Pore size distribution at lower airfoil cross-section.

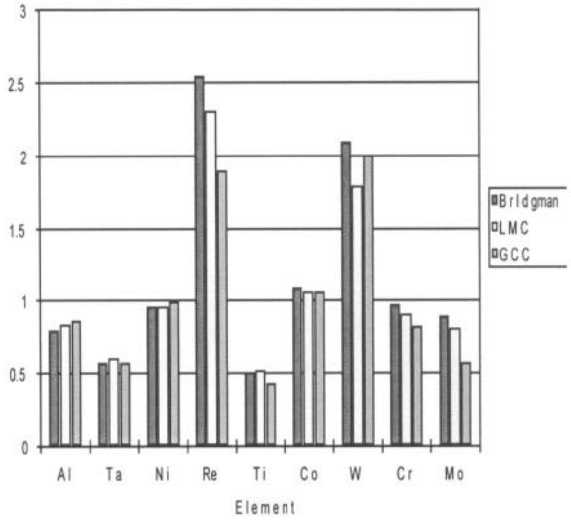

Fig. 13: Dendritic segregation of elements in as-cast condition vs. casting technique.

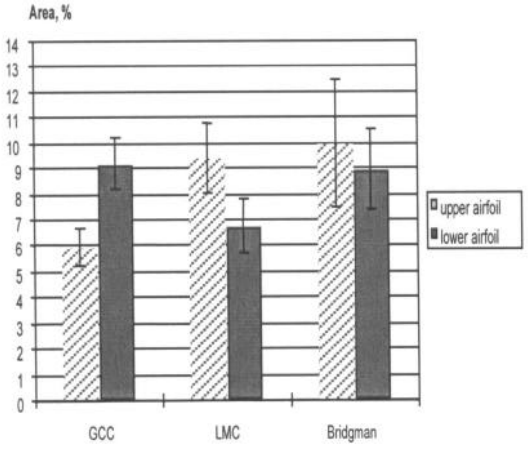

Fig. 12: Eutectic area fraction for different casting techniques.

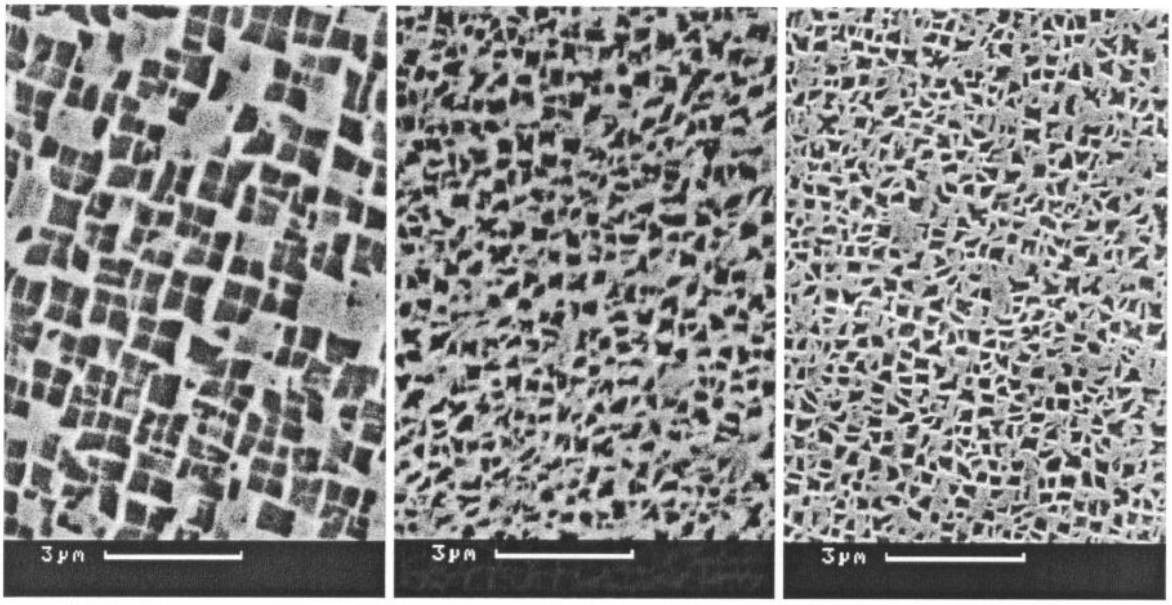

Bridgman LMC - Al GCC

Fig.. 14: Microstructure of as-cast SX alloy (MK-4) after various casting processes.